Environ Geochem Health (2024) 46:92
https://doi.org/10.1007/s10653-024-01871-1

ORIGINAL PAPER

Hydrothermal synthesis and photocatalytic application of ZnS-Ag composites based on biomass-derived carbon aerogel for the visible light degradation of methylene blue

Paramasivam Shanmugam · Balaji Parasuraman · Supakorn Boonyuen · Pazhanivel Thangavelu · Mohamad S. AlSalhi · Alvin Lim Teik Zheng · A. Viji

Received: 28 November 2023 / Accepted: 12 January 2024 / Published online: 17 February 2024

Abstract A facile and cost-effective hydrothermal followed by precipitation method is employed to synthesize visible light-driven ZnS-Ag ternary composites supported on carbon aerogel (CA). Extensive studies were conducted on the structural, morphological, and optical properties, confirming the successful formation of ternary nanocomposites. The obtained results evidently demonstrate the successful loading of ZnS and Ag onto the surface of the CA. High-resolution transmission electron microscopy analysis revealed that ZnS and Ag nanoparticles (AgNPs) were uniformly distributed on the surface of the CA with an average diameter of 18 nm. The biomass-derived CA, containing a hierarchical porous nano-architecture and an abundant number of $–NH_2$ functional groups on the surface, can greatly prevent the agglomeration, stability and reduce particle size. Brunauer–Emmett–Teller analysis results indicated specific surface areas of 4.62 $m^2\ g^{-1}$ for the CA, 48.50 $m^2\ g^{-1}$ for the CA/ZnS composite, and 62.62 $m^2\ g^{-1}$ for the CA/ZnS-Ag composite. These values demonstrate an increase in surface area upon the incorporation of ZnS and Ag into the CA matrix. Under visible light irradiation, the synthesized CA/ZnS-Ag composites displayed remarkably improved photodegradation efficiency of methylene blue (MB). Among the tested samples, the CA/ZnS-Ag composites exhibited the highest percentage of photodegradation efficiency, surpassing ZnS, CA, and CA/ZnS. The obtained percentages of degradation efficiency for CA, ZnS, CA/ZnS, and CA/ZnS-Ag composites were determined as 26.60%, 52.12%, 68.39%, and 98.64%, respectively. These results highlight the superior photocatalytic performance of the CA/ZnS-Ag composites in the degradation of MB under visible light conditions. The superior efficiency of the CA/ZnS-Ag composite can be attributed to multiple factors, including its elevated specific surface area, inhibition of electron–hole pair recombination, and enhanced photon absorption within the visible light spectrum. The CA/ZnS-Ag composites displayed

P. Shanmugam · S. Boonyuen (✉)
Department of Chemistry, Faculty of Science and Technology, Thammasat University, Pathum Thani 12120, Thailand
e-mail: chemistrytu@gmail.com

B. Parasuraman · P. Thangavelu
Smart Materials Laboratory, Department of Physics, Periyar University, Salem, Tamilnadu 636011, India

M. S. AlSalhi
Department of Physics and Astronomy, College of Science, King Saud University, P. O. Box 2455, 11451 Riyadh, Saudi Arabia

A. L. T. Zheng
Department of Science and Technology, Faculty of Humanities, Management and Science, Universiti Putra Malaysia Bintulu Campus, Bintulu, Sarawak, Malaysia

A. Viji
Department of Physics, Kongunadu College of Engineering and Technology, Thottiyam, Tamil Nadu 621215, India

consistent efficiency over multiple cycles, confirming their stable performance, reusability, and enduring durability, thereby showcasing the robust nature of this composite material.

Graphical abstract

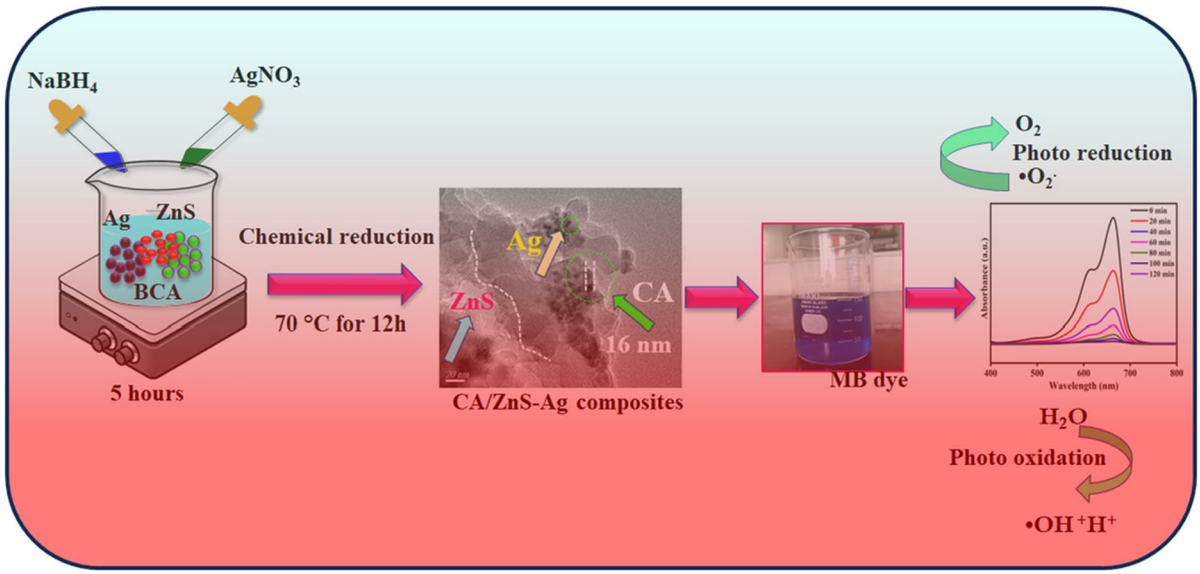

Keywords Carbon aerogel · CA/ZnS-Ag · Photocatalysts · Methylene blue · Recycling process

Introduction

The progress of industries and modern civilization has given rise to inevitable challenges concerning environmental contamination and energy scarcity (Fan et al., 2022; Ma et al., 2020). The leather, textile, paint, pharmaceutical and food processing industries are the main source of toxic substance release to the soil and water bodies (Ren et al., 2014). The industries released unwanted toxic chemicals and heavy metals to the environment, without any purification (Liu et al., 2019a, 2019b; Ngullie et al., 2022; Shanmugam et al., 2023a, 2023b; Vignesh et al., 2021). The water treatment is a crucial process designed to make water safe for various applications, including drinking, industrial processes, and environmental protection @@@(G et al., 2023; Haripriyan et al., 2022; Krishnan et al., 2023; Thanigaivel et al., 2022). The typical water treatment process involves several stages including coagulation and flocculation, sedimentation, filtration, disinfection, pH adjustment, softening, advanced oxidation process, adsorption and photocatalysts (Deng et al., 2023; Liu et al., 2024; Sivaranjani et al., 2023; Zhu et al., 2022). In recent years, advanced photocatalytic activity has become a proper technique with great potential for the degradation of organic dyes and water-spiting reactions (Aydoghmish et al., 2019; Subbulakshmi et al., 2023). Mostly, titanium oxide and zinc oxide semiconductor materials have been used to remove organic dyes from wastewater (Munusamy et al., 2023). However, materials have a wide band gap of 3.2 eV and have to use some limitations. These semiconductor materials used work under the UV light range, and then a small portion of UV light is only utilized in sunlight (Liu et al., 2019a, 2019b; Wang et al., 2018). Therefore, alternative semiconductor materials such as metal oxide, metal sulfide and carbon nitride operating under visible light are highly advised in this part (Raju et al., 2023; Ranjith et al., 2023a, 2023b; Ranjith et al., 2023a, 2023b; Shanmugam et al., 2023a, 2023b). Among them, metal sulfides such as Ag_2S,

CuS, CdS, ZnS, PbS and Sb_2S_3 have been exploited to remove the pollutants (Bharath et al., 2023; Li et al., 2021; Lu et al., 2018; Parasuraman et al., 2023a, 2023b; Prasad et al., 2020).

Particularly, ZnS has been a promising candidate for the removal of organic dyes, because of its toxic-free, easy method of preparation, strong oxidation and high conduction band (−0.9 eV) (Lu et al., 2018). However, photo corrosion, stability and lower efficiency of charge separation is a major disadvantage for the single-component system. In order to avoid these issues, add some foreign reagents into the ZnS (Prasad et al., 2020). Various types of strategies have been utilized to overcome these circumstances. For example, ZnS coupled, doping with one or more supporting materials (Mao et al., 2015; Sadaqat et al., 2021). Especially, carbon-based materials including graphene, carbon nanotubes, fullerene and carbon aerogel considered greater attention to enhance photocatalytic efficiency. Bharath and colleagues manufacture nanostructured materials consisting of reduced graphene oxide (rGO) supported Ru-$COFe_2O_4$, designed for high-performance photoelectrodes. These materials are employed to effectively convert hazardous Cr(VI) into less harmful Cr(III) through the process of anodic oxidation of phenols (Bharath et al., 2022). Particularly, biowaste-derived 3D carbon aerogel is a capable candidate for the preparation of CA/ZnS composites. The biomass-derived carbon aerogel (CA) have high porous in nature, non-toxic, high surface area, low density and ecofriendly, which creates a unique material for the efficient heterogeneous photocatalysts (Shanmugam et al., 2019; Zhang et al., 2023a, 2023b).

Furthermore, carbon aerogel shares similar properties with graphene and carbon nanotube, but its preparation cost is more economical when compared to graphene and carbon nanotube (Zhang et al., 2023a, 2023b). Prasad et al. reported the rod-shaped CdS/carbonaceous aerogel for the efficient photodegradation of methylene blue (Prasad et al., 2020). Fan et al. explored the application of chitosan-based aerogel-supported TiO catalysts for the removal of high concentrations of surfactants. This study not only offers a theoretical foundation but also provides technical support for the advancement of a technology designed to address high-concentration organic pollutants (Fan et al., 2023). Li et al. reported the photodegradation of organic dyes using 3D porous aerogel with tungsten oxide nanowires (Li et al., 2014). Similarly, Jin et al. also investigated TiO_2/CA as a photocatalyst for the removal of organic dyes (Jin et al., 2011). The incorporation of silver nanoparticles (AgNPs) into ZnS/CA composites serves several purposes, including increasing the surface area, alter the band gap and preventing the recombination of electron–hole pairs. These two factors primarily contribute to enhancing the photocatalytic activity (Sacco et al., 2019; Venugopal et al., 2023). It was reported that noble metals such as Ag, Au, Pt and Pd could act as efficient co-catalysts and enhance photocatalytic activity (Govarthanan et al., 2014; Sacco et al., 2019). Samaneh et al. reported the ultra-sound-assisted Ag-ZnS/rGO composites for the photodegradation of TC under visible light irradiation (Kameli & Mehrizad, 2019). Therefore, based on the above contents, the present study aims to fabricate Ag-ZnS nanoparticles immobilized onto the surface of biomass-derived 3-D carbonaceous aerogel to degrade the MB in an aqueous medium. Particularly, the carbon aerogel has low density and high porosity materials; good scoffold material for formation of composite. The light weight composites partially float on the surface of wastewater. This helps improve visible light adsorption. Furthermore, the carbon aerogel has a larger number of hydroxyl and amine groups; thus, these functional groups help attract dye molecules and create more contact between the catalyst surface and dye molecules. Based on the earlier literature, there is no reports for the synthesis of CA/ZnS-Ag composites for the photodegradation of MB. This process is well suited to large-scale production compared to existing chemical processes.

Experimental

Materials

All reagents were of analytical grade and utilized directly without extra purification. The chitosan was purchased from Merck, Germany. Silver nitrate ($AgNO_3$), zinc nitrate hexahydrate ($Zn(NO_3)_{2.6}H_2O$, sodium sulfide (Na_2S) and methylene blue (MB) were purchased from Research laboratories. Ethanol,

methanol, and acetone were purchased from Winnex co. Ltd.

Preparation of CA/ZnS composites

The CA was synthesized according to the earlier reported synthetic procedure (Shanmugam et al., 2019). During this procedure, 2 g of chitosan was introduced to 100 mL of deionized water within a 100-ml beaker. The resulting solution underwent dispersion through an ultrasonication process. Subsequently, the homogeneous mixture was transferred from the beaker to a 100-mL Teflon-lined autoclave. The sealed autoclave was subjected to heating at 180 °C for 12 h. Following the autoclave's cooling to room temperature, the reaction mixture underwent filtration and multiple washes with a deionized water–ethanol mixture to eliminate any remaining unreacted impurities. The carbonaceous aerogel (CA) was then acquired through a 36-h freeze-drying process utilizing a high-vacuum freeze-drying apparatus set at − 51 °C.

The obtained CA was used as a scaffold candidate for the CA/ZnS composites. By this method, CA/ZnS composites were prepared by the precipitation method (Lu et al., 2018). In a detailed procedure, the 25 mL of Zn $(NO_3)_2{\cdot}6H_2O$ (5 mM, 1.49 g) solution was dissolved in a 100 mL beaker. The required amount of CA was immersed into the Zn $(NO_3)_2{\cdot}6H_2O$ solution. After that, 5 mM of Na_2S was added drop by drop. The whole reaction mixture was transferred into a stainless-steel autoclave and maintained at 180 °C for 18 h. The resulting reaction mixture was washed with ethanol and water to remove the soluble impurities. The CA/ZnS composites were obtained by lyophilized at − 51 °C for 36 h.

Preparation of CA/ZnS-Ag composites

The synthesis of CA/ZnS-Ag composites was carried out using self-assembly and chemical reduction procedures (Gong et al., 2021). Typically, 0.5 g of CA/ZnS composites were dispersed into the water and 10 ml of 0.01 mol of $AgNO_3$ solution was added drop by drop with continuous magnetic stirring. The Ag^+ ions were deposited/exploited on the CA/ZnS composites, after then add 0.01 M of $NaBH_4$ (10 mL) drop by drop and stirred continuously at 5 h. The resulting CA/ZnS-Ag composite was washed, centrifuged with H_2O/EtOH mixture, and finally dried at 70 °C overnight.

Photocatalytic study

The comparative photocatalytic activity of the as-prepared photocatalysts, viz., CA, ZnS, CA/ZnS and CA/ZnS-Ag were examined by photodegradation of MB dye under the UV–visible illustration method via a simple photocatalytic setup. In a typical experiment, 20 mg of photocatalysts was immersed into 30 mL of simulated organic dye pollutant (20 ppm), stirring for 30 min to achieve the adsorption–desorption equilibrium. 500 W halogen lamp was used as a light source for the photodegradation of MB dye. After the adsorption–desorption equilibrium, the reaction mixture was placed under light irradiation. During the simulated light irradiation, at a particular time of interval, 3 mL of dye solution was taken out to remove the catalysts using centrifugation. The centrifugate was analyzed by a UV–visible spectrophotometer. The percentage of degradation efficiency of MB has been calculated according to Eq. (1) (Mohamed et al., 2018).

$$\%\ \text{of degradation efficiency} = C_0 - C/C_0 \times 100 \quad (1)$$

Characterizations

The XRD pattern of the CA/ZnS-Ag were analyzed with X-ray diffraction (XRD, Bruker D8 advanced diffractometry, Japan) with Cu K ($\lambda = 1.54$ A°). The internal morphologies CA/ZnS-Ag composites were studied by high-resolution transmission electron microscopy (HR-TEM, JOEL-JEM-2100, Japan). Fourier transform infrared spectra (FTIR) were recorded on a Nicolet iS5 (Thermo Fisher Scientific, Madison, WI, USA). The specific surface area of the prepared CA, CA/ZnS and CA/ZnS-Ag were analyzed by Brunauer–Emmett–Teller (BET) and was carried out by N_2 adsorption desorption. The energy bandgaps of the prepared samples were performed by utilizing DRS-UV spectrophotometer SHIMADZU 3600 (SHIMADZU, Kyoto, Japan) (Scheme 1).

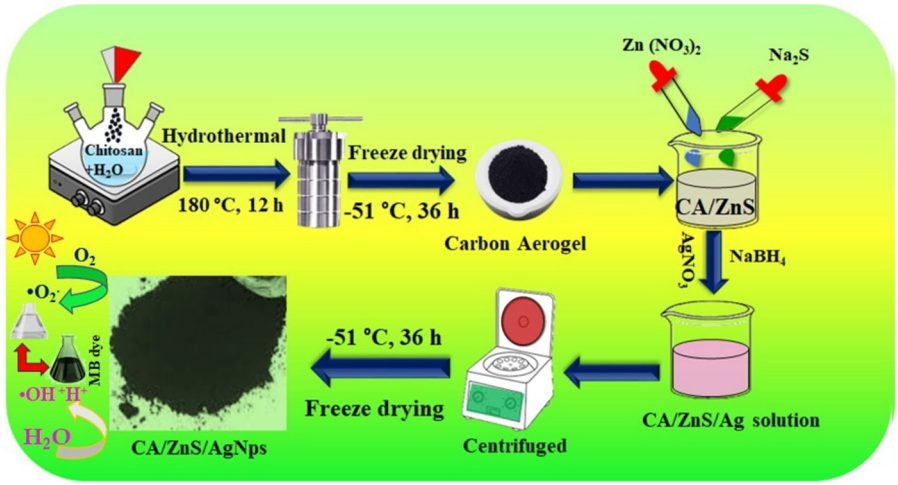

Scheme 1 Schematic illustration of the synthesis of CA/ZnS-AgNPs composites for the photodegradation of methylene blue

Results and discussion

Characterization of synthesized photocatalysts

To assess the crystallinity of the as-prepared pure CA, ZnS and CA/ZnS-Ag composites were characterized by X-ray diffraction (XRD) (Fig. 1a, b). In Fig. 1a, the XRD pattern of CA, the broad peak appeared at 20.21° which is attributed to carbon (002) plane graphite-like structure (JCPDS. NO: 75-1621) (Fatnassi et al., 2022; Prasad et al., 2020). Further, the XRD spectrum of ZnS shows that the observed diffraction peaks at 28.61°, 33.20°, 47.61°, 56.41°, 69.55° and 76.81° exhibit corresponding to the crystal lattices (111), (200), (220), (311), (400) and (331), respectively (JCPDS. No: 05-0566) (Fig. 1b) (Dixit & Soni, 2014; Lu et al., 2018). Additionally, similar peaks appeared at CA/ZnS-Ag composites, thus confirming the formation of CA/ZnS-Ag composites. Compared with ZnS and CA/ZnS-Ag composites, the peak intensity of the CA/ZnS-Ag composites slightly decreased, which is due to CA and Ag NPs. Further, there is no additional peaks appearing at CA/ZnS-Ag composites, thus reveals that AgNPs does not alter the crystallinity of ZnS. The average crystalline was calculated by three different major peaks using Scherrer's equation. The obtained crystalline values are 27 nm and

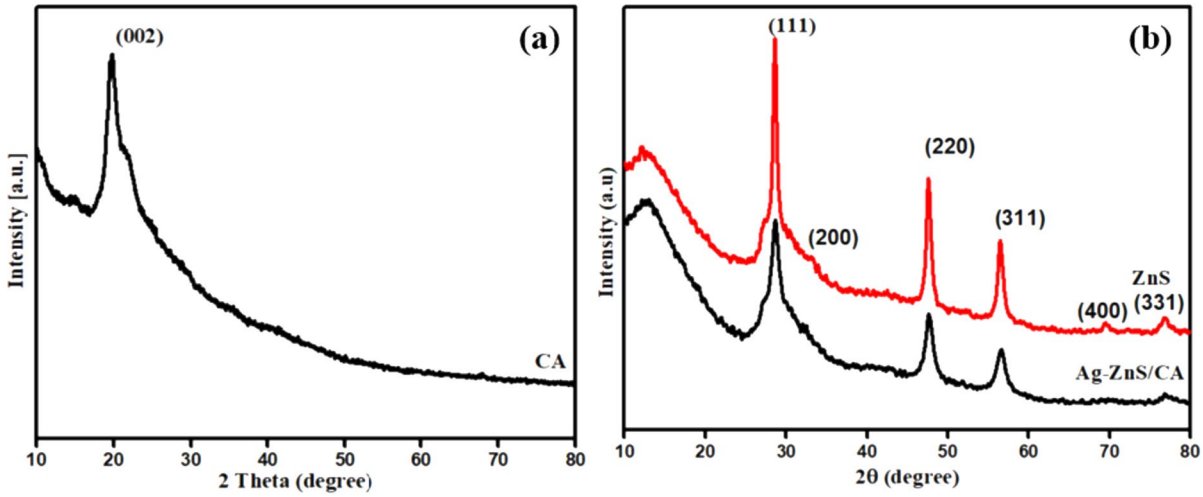

Fig. 1 XRD pattern of the **a** CA and **b** ZnS, CA/ZnS-Ag composites

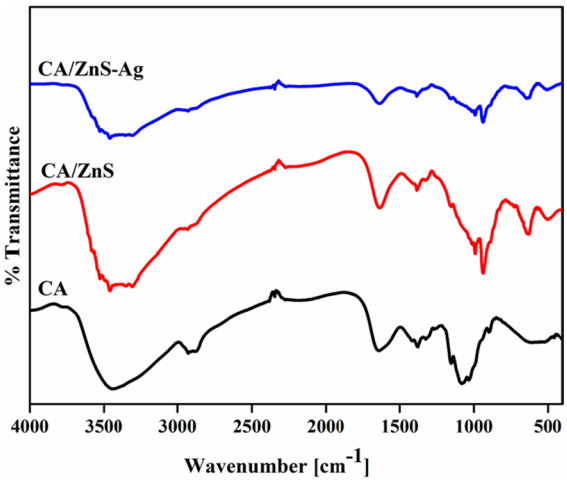

Fig. 2 FTIR spectrum of the CA, CA/ZnS and CA/ZnS-Ag composites

15 nm for ZnS and Ag-CA/ZnS composites. The particle size was decreased in the composites, and the CA contained a larger number of functional organic functional groups, thus stabilizing and reducing the particle size.

Figure 2 represents the detailed structural evolution of the FTIR spectra of the CA, CA/ZnS and CA/ZnS-Ag composites. In CA, the typical absorption peaks appeared at 3447.04, 2890.99, 1635.05, 1155.57 and 1086.74 cm^{-1} corresponding to OH, $–NH_2$, $–CH_2$, –C=O, C–C and C–O–C, respectively (Lu et al., 2018). The larger number of –OH and $–NH_2$ which helps to prevent the aggregation and reducd the particles size, noticed in TEM images (Ren et al., 2014). This peak evidence confirmed the prepared carbon aerogel contains a larger number of functional groups, thus supporting/stabilizing the Ag and ZnS nanoparticles (Patel et al., 2017). The biomass-derived carbon aerogel, containing an abundant number of $–NH_2$ and –OH functional groups on the surface, can significantly prevent agglomeration, enhance stability and reduce particle size. Thus, it enhances the surface area of the composites (Ren et al., 2014). The characteristic peaks of the CA peak appeared at the CA/ZnS composites, additionally, the strong band at 644.43 cm^{-1} is due to the Zn–S bond (Parasuraman et al., 2023a, 2023b). Thus, peak evidence gave the additional confirmation of ZnS nanoparticles strongly bound into the CA. In FTIR spectrum of CA/ZnS-Ag composites, the peaks intensity

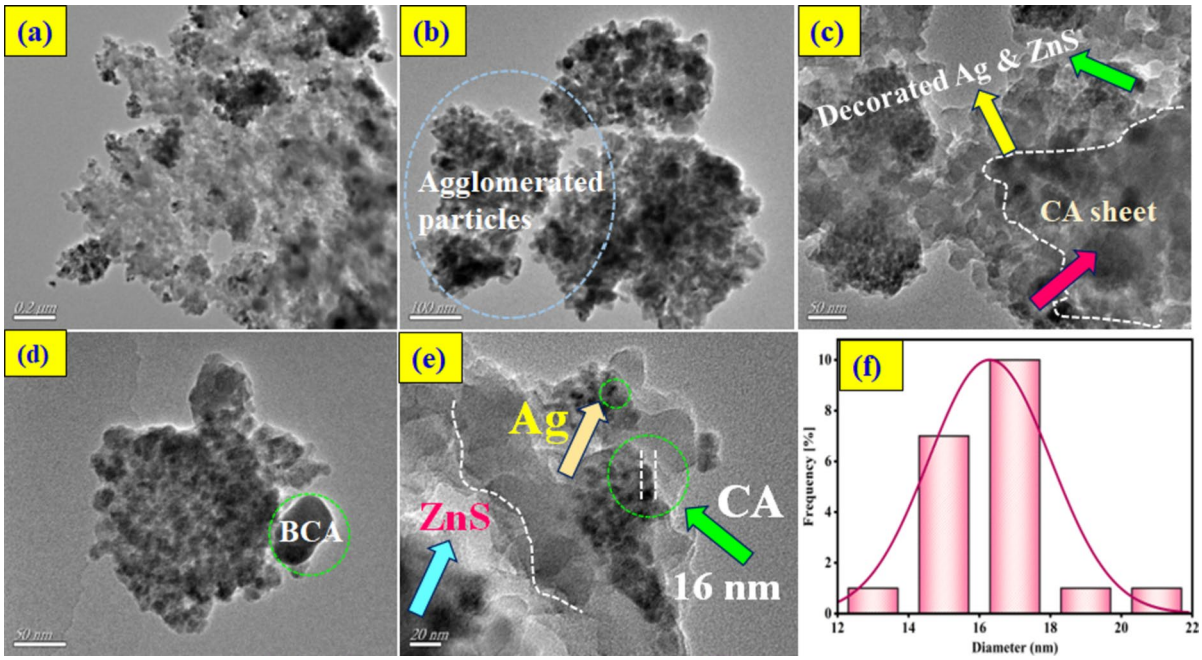

Fig. 3 **a–c** HRTEM images of the CA/ZnS-Ag composites, **d** particle size distribution histogram curve of the CA/ZnS-Ag composites

of CA functional groups are reduced and slightly shifted after addition of AgNPs.

Further, the size and morphology of the prepared CA/ZnS-Ag composites were exploited by TEM analysis as shown in Fig. 3a–e. As shown in Fig. 3a, b, the nano-structured ZnS is evenly distributed onto the surface of three-dimensional CA (Lu et al., 2018; Yan et al., 2015). Further, in Fig. 3c–d, a very tiny block dots appear in ZnS and CA composites, thus AgNPs. Moreover, the Ag and ZnS NPs are evenly distributed onto the CA. additionally, Fig. 3e, shows that, ZnS and AgNPs decorated onto the surface of CA layer and thus improve the surface area and reflect the photocatalytic activity. To using the HRTEM images to plot the particle size distribution histogram curve, it was found that the Ag-ZnS are evenly distributed onto the CA, the average particle size was around 12–18 nm (Fig. 3f). The similar results existence with the XRD results.

The specific surface area is one of the key parameter for the catalytic activity. The specific surface area, pore volume and diameter of the CA, CA/ZnS and CA/ZnS-Ag were measured by BET-nitrogen adsorption–desorption isotherm. As shown in Fig. 4 displays the N_2 adsorption–desorption isotherms with H_2-type hysteresis loop in the range of 0.5–0.8, which is characteristic of mesoporous structure with interconnected pores (according to IUPAC classification) (Thommes & Cychosz, 2014). The textural properties of CA, CA/ZnS and CA/ZnS-Ag composites

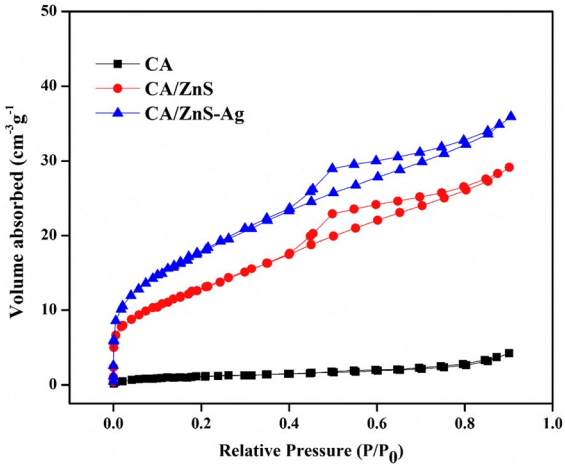

Fig. 4 Nitrogen adsorption–desorption isotherms of different prepared CA, CA/ZnS and CA/ZnS-Ag composites

Table 1 Photodegradation efficiency and rate constant of the prepared samples for MB dye

S. no	CA	ZnS	CA/ZnS	CA/ZnS-Ag
K_{obs}	0.0024	0.0053	0.009	0.01795
R^2	0.9865	0.9901	0.9745	0.9901
Degradation efficiency (%) (150 min)	26.59	52.11	68.29	98.64
Surface area (m^2g^{-1})4	4.62	–	48.50	62.62
Pore volume (cm^3g^{-1})	0.0065	–	0.045	0.0558
Pore diameter (nm)	5.6	–	3.71	3.35

are given in Table 1. The surface area of the prepared CA, CA/ZnS and CA/ZnS-Ag composites are 4.62 m^2/g, 48.50 m^2/g and 62.22 m^2/g, respectively. The CA/ZnS-Ag composites have higher surface area than CA/ZnS and CA, the AgNPs enhance the surface area of the CA/ZnS, which can favor the adsorption of reactants and provide more reactive sites, thus improving the photocatalytic activity. Further, the pore volume of the prepared samples is 0.0065 cm^3/g, 0.045 cm^3/g and 0.0558 cm^3/g for CA, CA/ZnS and CA/ZnS-Ag, respectively. Additionally, the pore diameter of the CA for 5.6 nm, CA/ZnS for 3.71 nm and CA/ZnS-Ag for 3.35 nm, respectively.

Figure 5a shows the optical properties of as-prepared samples, viz., CA, ZnS, CA/ZnS, and CA/ZnS-Ag composites. The option absorption edge of the pure ZnS and CA was found to be 342 nm and 334 nm, respectively. The energy band gap of the prepared composites was calculated by Tauc plot using energy dependency correlation of $ahn=(hn-Eg)^{1/2}$, where a and Eg represent the absorption coefficient and energy band gap of the synthesized composites (Fig. 5b), respectively. The estimated energy bandgap values are 3.3 eV for CA and 3.1 eV for ZnS, respectively, which is in good agreement with the earlier literature (Jeyaram et al., 2017). Moreover, composite materials such as CA/ZnS and CA/ZnS-Ag exhibited a broader absorption peak at visible regions in the range of 400–580 nm. This CA and AgNPs modified the ZnS bandgap and reduced the electron–hole pair recombination. Further, a positive synergetic effect occurred on ZnS and CA thus enlarging photon absorption which lead to excellent photocatalytic activities (Lu et al., 2018; Xu et al.,

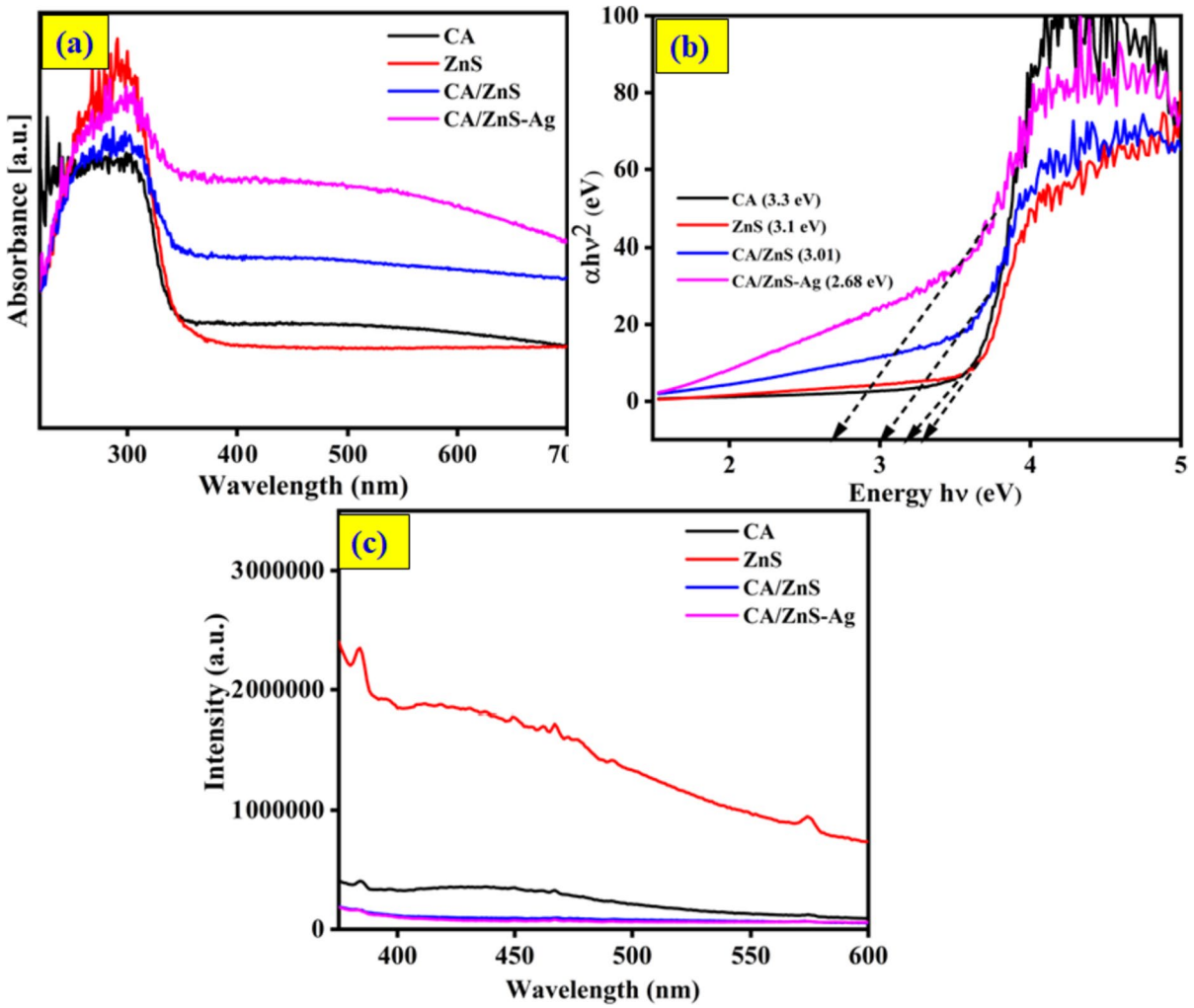

Fig. 5 **a** UV−Vis absorption spectrum, **b** Tacu plot and **c** PL spectra of CA, ZnS, CA/ZnS and CA/ZnS-Ag composites

2014). The bandgap for the CA/ZnS and CA/ZnS-Ag composites materials was estimated to be 3.01 and 2.68 eV, respectively. These results reveal that the energy bandgaps are reduced in the composite materials due to the positive synergetic effect occurring on Ag, ZnS, and CA (Selvi et al., 2021).

Figure 5c shows the PL spectra of the CA, ZnS, CA/ZnS, and CA/ZnS-Ag composites with a maximum emission peak appearing at 454 nm with an excitation wavelength of 350 nm. In comparison with CA, ZnS, and CA/ZnS, the CA/ZnS composite materials had the weakest peak intensity, thus indicating that heterojunction was beneficial for enhancing the separation efficiency of photogenic carriers and photocatalytic performance. Furthermore, the CA/ZnS and CA/ZnS-Ag composites, the Ag-loaded CA/ZnS had a low peak intensity, which is due to a metal–dipole quenching effect (Kim et al., 2014; Park et al., 2014). The lower intensity peak values of CA/ZnS-Ag have the highest photocatalytic performance (Messalti et al., 2021; Wang et al., 2015).

Photocatalytic activity

The comparative photocatalytic efficiency of the as-prepared CA, ZnS, CA/ZnS, and CA/ZnS-Ag composites was examined through the degradation of methylene blue (MB) under visible light illumination. In this degradation study, pure ZnS, CA, and ZnS-AgNPs were used as references for comparison. The

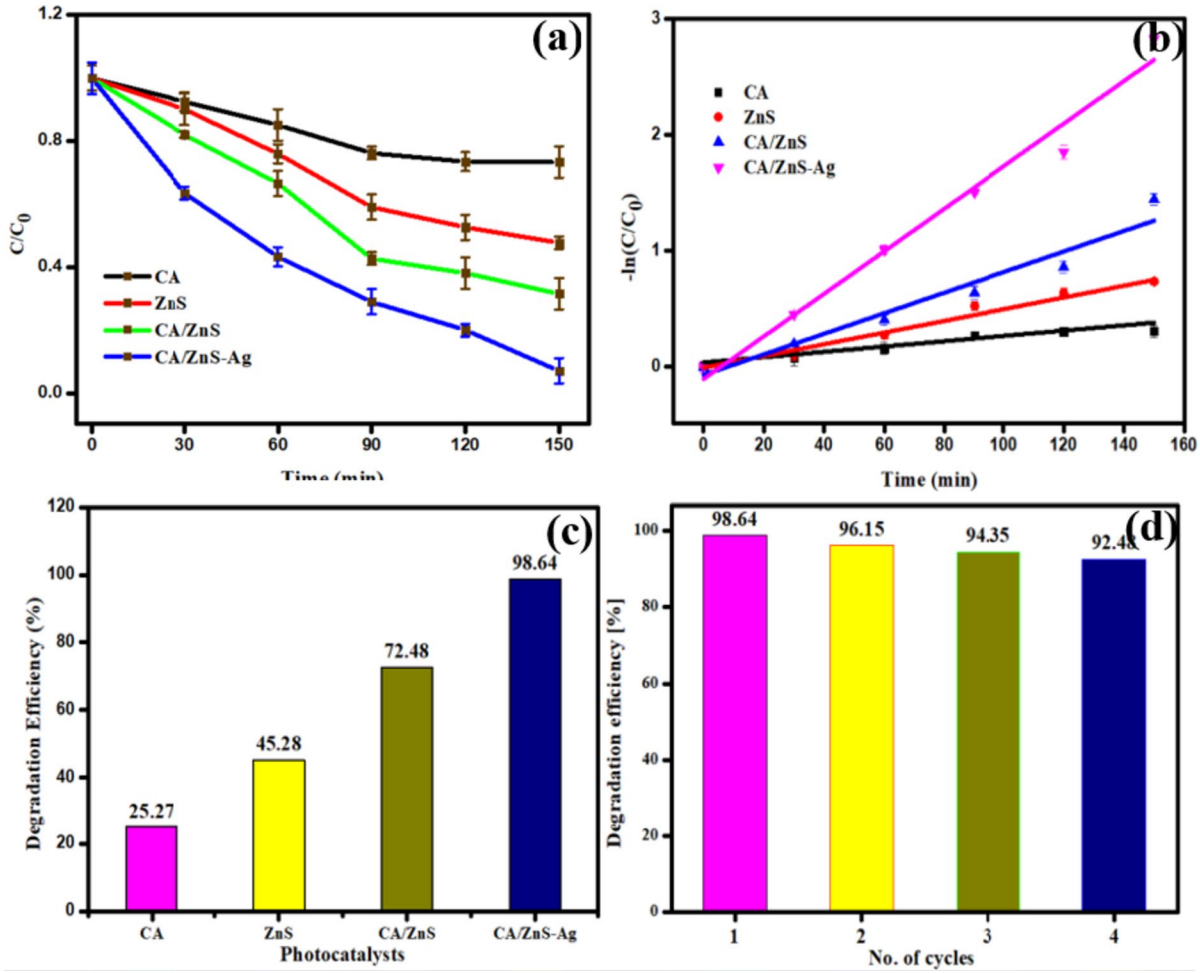

Fig. 6 **a** Photocatalytic degradation of MB dye and **b** Pseudo first-order kinetic plots of the as-prepared CA, ZnS, CA/ZnS and CA/ZnS-Ag composites, **c** degradation efficiency of the prepared samples and **d** Recycling efficiency of the CA/ZnS-Ag composites for MB degradation

initial concentration of MB was determined through maximum absorption measurements using UV–Vis spectroscopy (Fig. 6). The reaction mixture was kept under visible light irradiation, and in the absence of catalysts, no changes occurred in the concentration of MB dye. After the addition of catalysts, the reaction mixture was kept under dark conditions, and the concentration was measured using UV–Vis spectroscopy. The obtained results reveal that there were no significant concentration changes in MB; only trace amounts of MB were absorbed onto the surface of photocatalysts. The concentration of MB dye gradually decreased under visible light irradiation in the presence of photocatalysts. Further, the photocatalytic efficiency of the CA and ZnS shows lower degradation efficiency. Moreover, after addition of CA/ZnS and CA/ZnS-AgNPs was gradually increased, thus reveals that CA and AgNPs influenced the photocatalytic activity, because of the enhanced visible-light absorption and suppressed recombination rate in comparison with pure ZnS. Further, after addition CA and AgNPs, the specific surface area of the CA/ZnS-AgNPs has been increased, thus enhanced the photocatalytic activity.

In Fig. 6a, the decrease in [MB] is faster and more predominant in CA/ZnS-Ag composites than in CA, ZnS, and CA/ZnS. The CA and AgNPs effectively inhibit the recombination of photo-generated charge

carriers and increase the absorption of light (Bhunia & Jana, 2014). Based on the results, the degradation efficiency was found to be 25.27%, 45.28%, 72.48%, and 98.64% for CA, ZnS, CA/ZnS, and CA/ZnS-AgNPs, respectively (Fig. 6c). Compared with CA, ZnS, CA/ZnS, and CA/ZnS-Ag composites, the CA/ZnS-Ag composites achieved a degradation efficiency of 98.64% within 150 min (Subbulakshmi et al., 2023; Venugopal et al., 2023). As shown in Fig. 4b, the plots of the $\ln(C/C_0)$ versus time were liner, which indicates that the photodegradation of MB went through pseudo first order reaction. The k_{app} and R^2 values of degradation of MB as shown in Table 1. The obtained results reveal that the CA/ZnS-Ag composites exhibit a higher rate constant than CA, ZnS and CA/ZnS composites. The obtained rate constant value of CA/ZnS-Ag is 7.26-fold, 3.4-fold, and two-fold greater than CA, ZnS and CA/ZnS, respectively. Further, to test the catalysts stability/recycling efficiency of the CA/ZnS-Ag composites was carried out, the degradation of MB was under UV–Vis light irradiation (Fig. 6). The catalysts demonstrate good stability, and there is no loss of activity observed after five consecutive cycles. In Table 2, you can find the listed maximum degradation efficiency values for MB, and previous experimental results are included to enhance comprehension.

Tentative mechanism of photocatalysts

Figure 7 illustrates the photocatalytic degradation of CA/ZnS-Ag, both with and without the introduction of scavengers. The inclusion of scavengers, namely IPA, BQ and $AgNO_3$, leads to degradation percentage of 23%, 29% and 70% for CA/ZnS-Ag, respectively. Initially, the addition of IPA reduces degradation from 98.64 to 23% by capturing the holes. Similarly, with the addition of BQ and $AgNO_3$ significantly

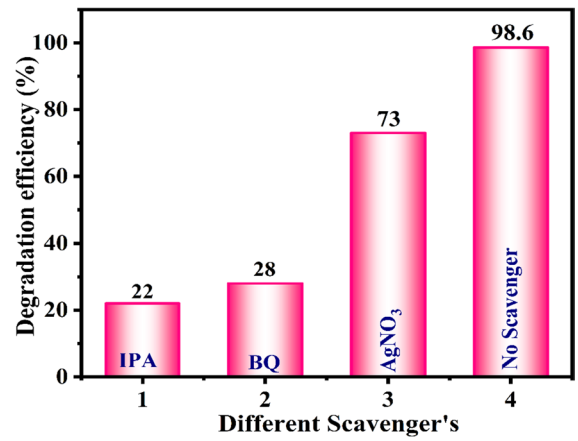

Fig. 7 Photodegradation ability of CA/ZnS-Ag with and without scavenger

diminishes the photocatalytic degradation of the MB dye, suggesting that BQ captures superoxide radical anions, whereas $AgNO_3$ captures electrons. Catalysts without any scavengers exhibit enhanced degradation performance due to the generation of a greater number of reactive active species under UV light exposure. These active species follow the order contributes the following order: $h^+ > O_2\cdot- > e^-$.

According to the experimental evidence, Fig. 8 illustrates the suggested photocatalytic mechanism for the prepared CA/ZnS-Ag composites. The mechanism of wide band gap semiconductors in the presence of visible light irradiation is comparatively challenging compared to typical semiconductors, as stated in the literature (Aruljothi et al., 2023; Kandasamy et al., 2023). When the CA/ZnS-Ag composites are exposed to visible light, CA can be stimulated. This means that the direct excitation of electrons from the valence band (VB) to the conduction band (CB) does not occur under VLI. Instead, the formation of

Table 2 Comparisons of photocatalytic performance towards MB with previous reports

Samples	Quantity of MB (mg/L)	Dosage of photocatalysts (mg)	Photocatalytic duration	Degradation efficiency	References
ZnS/rGO	10	20	180	75.02	Palve and Kokil (2019)
ZnS–RGO	3.2	20	60	98.98	Feng et al. (2013)
ZnS/CA	40	40	180	91.00	Lu et al. (2018)
ZnS–TiO_2/RGO	20	20	60	90.00	Qin et al. (2019)
CA/ZnS-Ah	10	10	150	98.64	This study

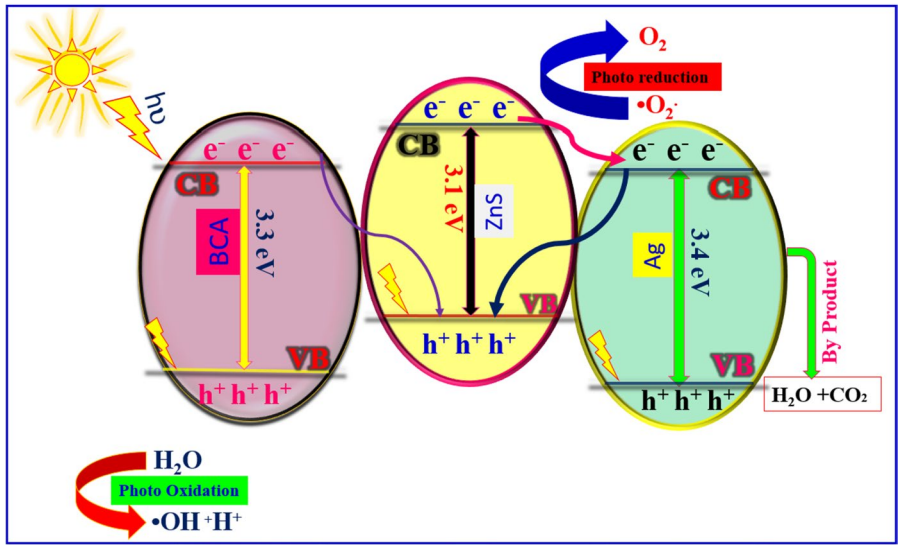

Fig. 8 Photodegradation mechanism of MB by CA/ZnS-Ag composites irradiated by visible light

electron–hole (e^{-}-h+) pairs takes place indirectly in the presence of a sacrificial agent. The experimental results indicate that CA and Ag play a crucial role in enhancing ZnS activity. In fact, the surface of CA acts as a photosensitizer, which is activated by VLI. Consequently, the released electrons from the CA surface are injected into the CB of ZnS or trapped by oxygen molecules, leading to the production of superoxide anion radicals ($^{\circ}O_2^{-}$). Alternatively, the positively charged CA can receive electrons from the CB of ZnS, resulting in the formation of photo-induced electron holes. Moreover, the excited Ag electrons under VLI can be shared through the surface plasmon resonance (SPR) effect with the CB of ZnS, generating photo-induced electrons. Following these steps, the photo-induced $e^{-}-h+$ pairs migrate to the photocatalytic surface. Additionally, water molecules (H_2O) are adsorbed on the photocatalysts, forming hydroxide anions (OH^{-}), while simultaneously dye molecules are adsorbed on the surface of the catalysts.

Conclusion

The biomass derived carbon aerogel supported CA/ZnS-Ag composites were successfully synthesized by hydrothermal process and low-cost precursors. The biomass derived carbon aerogel have several significant properties and potential applications, making them an area of interest in scientific research an various industries. The carbon aerogel derived composites improve the properties such as high surface area, prevention of aggregation, low density, high porosity, high thermal and electrical conductivity. The as-prepared CA, ZnS, CA/ZnS and CA/ZnS-Ag composites were confirmed by the various spectroscopic techniques such as XRD, FTIR, TEM, BET and UV–Vis analysis. The HRTEM results evidenced that, Ag and ZnS NPs evenly distributed onto the surface of CA, the average particles size was found to be 12–18 nm. Compared with CA and ZnS, the composite materials have a more specific surface area due to the surface functional group of CA reducing the particle size to enhance the specific surface area. The CA/ZnS-Ag composites achieved highest degradation efficiency (98.64%) within 150 min. Further, CA/ZnS-Ag had excellent catalytic stability, there is no loss of activity noticed after five consecutive recycling processes. The enhanced photocatalytic activity could be attributed to its large specific surface area, heterojunction between CA and AgNPs, which effectively prevents the recombination of photo-induced carriers and improves the absorption of visible light. Therefore, biomass derived carbon aerogel supported Ag-ZnS composites had a high photodegradation property, chemical stability, recycling property, non-toxicity, and had broad applications options in environmental applications.

Acknowledgements The authors gratefully acknowledge the Thammasat University Postdoctoral Fellowship (B.E.2564), Thailand Science Research and Innovation Fundamental Fund fiscal year 2023. The authors express their sincere appreciation to the Researchers Supporting Project Number (RSP2024R68) King Saud University, Riyadh, Saudi Arabia.

Author contribution PS contributed to conceptualization, investigation, writing—original draft and visualization. SB done supervision, data curation, project administration and writing—review and editing. BP performed validation, review and editing, PT and MSA done review and resources, ALTZ done review and editing and VA done data curation and formal analysis.

Funding Not applicable.

Data availability Data will be made available on request.

Declarations

Conflict of interest The authors declare no competing interests.

Ethical approval Not applicable.

Consent to participate Not applicable.

Consent for publication Not applicable.

References

Aruljothi, C., Balaji, P., Vaishnavi, E., Pazhanivel, T., & Vasuki, T. (2023). Magnetic recyclable $CuFe_2O_4$/rGO nanocomposite for the degradation of tetracycline under sunlight irradiation. *Journal of Chemical Technology and Biotechnology, 98*(8), 1908–1917. https://doi.org/10.1002/jctb.7408

Aydoghmish, S. M., Hassanzadeh-Tabrizi, S. A., & Saffar-Teluri, A. (2019). Facile synthesis and investigation of NiO–ZnO–Ag nanocomposites as efficient photocatalysts for degradation of methylene blue dye. *Ceramics International, 45*(12), 14934–14942. https://doi.org/10.1016/j.ceramint.2019.04.229

Banat, G. B. F., & Abu, H. M. (2023). Photoelectrochemical advanced oxidation processes for simultaneous removal of antibiotics and heavy metal ions in wastewater using 2D-on-2D WS_2@$CoFe_2O_4$ heteronanostructures. *Environmental Pollution, 339*, 122753. https://doi.org/10.1016/j.envpol.2023.122753

Bharath, G., Hai, A., Kiruthiga, T., Rambabu, K., Sabri, M. A., Park, J., et al. (2022). Fabrication of Ru–$CoFe_2O_4$/RGO hierarchical nanostructures for high-performance photoelectrodes to reduce hazards Cr(VI) into Cr(III) coupled with anodic oxidation of phenols. *Chemosphere, 299*, 134439. https://doi.org/10.1016/j.chemosphere.2022.134439

Bharath, G., Rambabu, K., Alqassem, B., Morajkar, P. P., Abu Haija, M., Nadda, A. K., et al. (2023). Fabrication of gold nanodots decorated on 2D tungsten sulfide (Au-WS_2) photoanode for simultaneous oxidation of phenol and arsenic (III) from industrial wastewater. *Chemical Engineering Journal, 456*, 141062. https://doi.org/10.1016/j.cej.2022.141062

Bhunia, S. K., & Jana, N. R. (2014). Reduced graphene oxide-silver nanoparticle composite as visible light photocatalyst for degradation of colorless endocrine disruptors. *ACS Applied Materials and Interfaces, 6*(22), 20085–20092. https://doi.org/10.1021/am505677x

Deng, J., Gu, Z., Wu, L., Zhang, Y., Tong, Y., Meng, F., et al. (2023). Efficient purification of graphite industry wastewater by a combined neutralization-coagulation-flocculation process strategy: Performance of flocculant combinations and defluoridation mechanism. *Separation and Purification Technology, 326*, 124771. https://doi.org/10.1016/j.seppur.2023.124771

Dixit, N., & Soni, H. P. (2014). Tuning optical properties of ZnS nanoparticles in micellar medium at different pH. *Superlattices and Microstructures, 65*, 344–352. https://doi.org/10.1016/j.spmi.2013.11.018

Fan, S., Chen, J., Tian, L., Fan, C., Xu, W., Zhang, Y., et al. (2023). Construction of a recyclable chitosan-based aerogel-supported TiO2 catalyst for treating high-concentration surfactants. *Composites Part b: Engineering, 251*, 110475. https://doi.org/10.1016/j.compositesb.2022.110475

Fan, T., Fu, T., Xu, Q., & Gjoni, G. (2022). Research on the purification of environmental pollution by biomaterials and its treatment methods in the development of rural cultural and creative industries. *Bioinorganic Chemistry and Applications, 2022*, e1594081. https://doi.org/10.1155/2022/1594081

Fatnassi, A., Cammarano, C., Oliviero, E., Hulea, V., & Brun, N. (2022). Carbon-aerogel-supported noble-metal nanoparticles as hydrogenation catalysts. *ACS Applied Nano Materials, 5*(10), 14227–14234. https://doi.org/10.1021/acsanm.2c03313

Feng, Y., Feng, N., Zhang, G., & Du, G. (2013). One-pot hydrothermal synthesis of ZnS-reduced graphene oxide composites with enhanced photocatalytic properties. *CrystEngComm, 16*(2), 214–222. https://doi.org/10.1039/C3CE41423J

Gong, H., Hajizadeh, S., Liu, W., & Ye, L. (2021). Imprinted polymer beads loaded with silver nanoparticles for antibacterial applications. *ACS Applied Bio Materials, 4*(3), 2829–2838. https://doi.org/10.1021/acsabm.1c00045

Govarthanan, M., Selvankumar, T., Manoharan, K., Rathika, R., Shanthi, K., Lee, K.-J., et al. (2014). Biosynthesis and characterization of silver nanoparticles using panchakavya, an Indian traditional farming formulating agent. *International Journal of Nanomedicine, 9*, 1593–1599. https://doi.org/10.2147/IJN.S58932

Haripriyan, U., Arun, J., Gopinath, K. P., Mythili, R., Kim, W., & Govarthanan, M. (2022). A mini-review on innovative

strategies for simultaneous microbial bioremediation of toxic heavy metals and dyes from wastewater. *Archives of Microbiology, 205*(1), 29. https://doi.org/10.1007/s00203-022-03367-x

Jeyaram, J., Varadharajan, K., Singaram, B., & Rajendhran, R. (2017). Optical, photoconducting, thermal and anisotropic mechanical behaviours of Benzimidazolium salicylate single crystals. *Journal of Science: Advanced Materials and Devices, 2*(4), 445–454. https://doi.org/10.1016/j.jsamd.2017.09.004

Jin, Y., Wu, M., Zhao, G., & Li, M. (2011). Photocatalysis-enhanced electrosorption process for degradation of high-concentration dye wastewater on TiO_2/carbon aerogel. *Chemical Engineering Journal, 168*(3), 1248–1255. https://doi.org/10.1016/j.cej.2011.02.026

Kameli, S., & Mehrizad, A. (2019). Ultrasound-assisted synthesis of Ag-ZnS/rGO and its utilization in photocatalytic degradation of tetracycline under visible light irradiation. *Photochemistry and Photobiology, 95*(2), 512–521. https://doi.org/10.1111/php.12998

Kandasamy, M., Vasudevan, V., Thangavelu, P., Parasuraman, B., Govindasamy, M., Habila, M. A., et al. (2023). Synthesis of a hybrid phase $FeCoWO_4$/g-C_3N_4 heterojunction composite for enhanced photocatalytic degradation of MB under visible light. *ChemistrySelect, 8*(45), e202302715. https://doi.org/10.1002/slct.202302715

Kim, W. J., Pradhan, D., Min, B.-K., & Sohn, Y. (2014). Adsorption/photocatalytic activity and fundamental natures of BiOCl and $BiOClxI_{1x}$ prepared in water and ethylene glycol environments, and Ag and Au-doping effects. *Applied Catalysis b: Environmental, 147*, 711–725. https://doi.org/10.1016/j.apcatb.2013.10.008

Krishnan, R. Y., Manikandan, S., Subbaiya, R., Karmegam, N., Kim, W., & Govarthanan, M. (2023). Recent approaches and advanced wastewater treatment technologies for mitigating emerging microplastics contamination—A critical review. *Science of the Total Environment, 858*, 159681. https://doi.org/10.1016/j.scitotenv.2022.159681

Li, J.-X., Zhang, R.-L., Pan, Z.-J., Liao, Y., Xiong, C.-B., Chen, M.-L., et al. (2021). Preparation of CdS@C photocatalyst using phytoaccumulation Cd recycled from contaminated wastewater. *Frontiers in Chemistry, 9*, 2154. https://doi.org/10.3389/fchem.2021.717210

Li, X., Yang, S., Sun, J., He, P., Xu, X., & Ding, G. (2014). Tungsten oxide nanowire-reduced graphene oxide aerogel for high-efficiency visible light photocatalysis. *Carbon, 78*, 38–48. https://doi.org/10.1016/j.carbon.2014.06.034

Liu, R., Yuan, J., Huang, L., Yu, S., Zhao, Y., Duan, C., & Jiang, H. (2024). Synergistic enhancement of coal slurry water sedimentation and dehydration process using PDMDAAC/PAM. *Journal of Cleaner Production, 434*, 140160. https://doi.org/10.1016/j.jclepro.2023.140160

Liu, X.-D., Chen, K., Ma, S., Hao, Z.-H., Liang, S., Zhou, L., & Wang, Q.-Q. (2019b). Synthesis of Au/CdSe Janus nanoparticles with efficient charge transfer for improving photocatalytic hydrogen generation. *Nanoscale Research Letters, 14*(1), 349. https://doi.org/10.1186/s11671-019-3185-6

Liu, X., Xu, J., Ni, Z., Wang, R., You, J., & Guo, R. (2019a). Adsorption and visible-light-driven photocatalytic properties of Ag_3PO_4/WO_3 composites: A discussion of the mechanism. *Chemical Engineering Journal, 356*, 22–33. https://doi.org/10.1016/j.cej.2018.09.001

Lu, J., Hu, H., Yang, S., Shanmugam, P., Wei, W., Selvaraj, M., & Xie, J. (2018). ZnS@carbonaceous aerogel composites fabricated in production of hydrogen and for removal of organic pollutants. *Journal of Materials Science: Materials in Electronics, 29*(10), 8523–8534. https://doi.org/10.1007/s10854-018-8866-x

Ma, L., Ai, X., Lu, Y., Yan, S., & Wu, X. S. (2020). Development of a new synthetic strategy for highly reduced graphene oxide-CdS quantum-dot nanocomposites and their photocatalytic activity. *Journal of Alloys and Compounds, 828*, 154406. https://doi.org/10.1016/j.jallcom.2020.154406

Mao, M., Jiang, L., Wu, L., Zhang, M., & Wang, T. (2015). The structure control of ZnS/graphene composites and their excellent properties for lithium-ion batteries. *Journal of Materials Chemistry A, 3*(25), 13384–13389. https://doi.org/10.1039/C5TA01501D

Messalti, A. S., El-Ghozzi, M., Zambon, D., Mahiou, R., & Setifi, Z. (2021). Investigating photoluminescence properties of Ca-doped ZnS nanoparticles prepared via hydrothermal method. *Journal of Luminescence, 238*, 118227. https://doi.org/10.1016/j.jlumin.2021.118227

Mohamed, M. J. S., Shenoy, U. S., & Bhat, D. K. (2018). Novel NRGO-$CoWO_4$-Fe_2O_3 nanocomposite as an efficient catalyst for dye degradation and reduction of 4-nitrophenol. *Materials Chemistry and Physics, 208*, 112–122. https://doi.org/10.1016/j.matchemphys.2018.01.012

Munusamy, S., Mandlimath, T.R., Swetha, P., Al-Sehemi, A.G., Pannipara, M., Koppala, S., Shanmugam, P., Boonyuen, S., Pothu, R., & Boddula, R. (2023). Nitrogen-doped carbon dots: Recent developments in its fluorescent sensor applications. *Environmental Research, 231*, 116046.

Ngullie, R. C., Bhuvaneswari, K., Shanmugam, P., Boonyuen, S., Smith, S. M., & Sathishkumar, M. (2022). Magnetically RECOVERABLE BIOMASS-DERIVED carbon-aerogel supported ZnO (ZnO/MNC) composites for the photodegradation of methylene blue. *Catalysts, 12*(9), 1073. https://doi.org/10.3390/catal12091073

Palve, A. M., & Kokil, D. N. (2019). One-pot synthesis of ZnS-rGO nanocomposites using single-source molecular precursor for photodegradation of methylene blue and reduction towards toxic Cr(VI) under solar light. *Materials Research Express, 6*(10), 105536. https://doi.org/10.1088/2053-1591/ab408f

Parasuraman, B., Kandasamy, B., Murugan, I., Alsalhi, M. S., Asemi, N., Thangavelu, P., & Perumal, S. (2023a). Designing the heterostructured $FeWO_4$/FeS_2 nanocomposites for an enhanced photocatalytic organic dye degradation. *Chemosphere, 334*, 138979. https://doi.org/10.1016/j.chemosphere.2023.138979

Parasuraman, B., Shanmugam, P., Govindasamy, P., Nangan, S., Gnanasekaran, L., & Thangavelu, P. (2023b). Photocatalytic degradation of tetracycline contaminated wastewater over Bi_2S_3/$BiWO_6$/rGO ternary nanocomposite

under visible light irradiation. *Journal of the Taiwan Institute of Chemical Engineers, 25*, 105249. https://doi.org/10.1016/j.jtice.2023.105249

Park, Y., Na, Y., Pradhan, D., Min, B.-K., & Sohn, Y. (2014). Adsorption and UV/Visible photocatalytic performance of BiOI for methyl orange, Rhodamine B and methylene blue: Ag and Ti-loading effects. *CrystEngComm, 16*(15), 3155–3167. https://doi.org/10.1039/C3CE42654H

Patel, K., Deshpande, M. P., & Chaki, S. H. (2017). Effect of Ag on structural, optical and luminescence properties of ZnS nanoparticles synthesized by microwave-assisted chemical route. *Applied Physics A, 123*(5), 367. https://doi.org/10.1007/s00339-017-0980-8

Prasad, S., Shanmugam, P., Bhuvaneswari, K., Palanisamy, G., Pazhanivel, T., Arunkumar, T., et al. (2020). Rod-shaped carbon aerogel-assisted CdS nanocomposite for the removal of methylene blue dye and colorless phenol. *Crystals, 10*(4), 300. https://doi.org/10.3390/cryst10040300

Qin, Y., Zhao, W., Sun, Z., Liu, X., Shi, G., Liu, Z., et al. (2019). Photocatalytic and adsorption property of ZnS–TiO_2/RGO ternary composites for methylene blue degradation. *Adsorption Science and Technology, 37*(9–10), 764–776. https://doi.org/10.1177/0263617418810932

Raju, M., Parasuraman, B., Govindasamy, P., Thangavelu, P., & Duraisamy, S. (2023). Improved anti-diabetic and anti-cancer activities of green synthesized CuO nanoparticles derived from Tabernaemontana divaricate leaf extract. *Environmental Science and Pollution Research*. https://doi.org/10.1007/s11356-023-26261-5

Ranjith, R., Karmegam, N., Alsawalha, M., Hu, X., & Jothimani, K. (2023a). Construction of g-C_3N_4/CdS/$BiVO_4$ ternary nanocomposite with enhanced visible-light-driven photocatalytic activity toward methylene blue dye degradation in the aqueous phase. *Journal of Environmental Management, 330*, 117132. https://doi.org/10.1016/j.jenvman.2022.117132

Ranjith, R., Vignesh, S., Balachandar, R., Suganthi, S., Raj, V., Ramasundaram, S., et al. (2023b). Construction of novel g-C_3N_4 coupled efficient Bi_2O_3 nanoparticles for improved Z-scheme photocatalytic removal of environmental wastewater contaminant: Insight mechanism. *Journal of Environmental Management, 330*, 117134. https://doi.org/10.1016/j.jenvman.2022.117134

Ren, Y., Xu, Q., Zhang, J., Yang, H., Wang, B., Yang, D., et al. (2014). Functionalization of biomass carbonaceous aerogels: Selective preparation of MnO_2@CA composites for supercapacitors. *ACS Applied Materials and Interfaces, 6*(12), 9689–9697. https://doi.org/10.1021/am502035g

Sacco, O., Vaiano, V., Sannino, D., Picca, R. A., & Cioffi, N. (2019). Ag modified ZnS for photocatalytic water pollutants degradation: Influence of metal loading and preparation method. *Journal of Colloid and Interface Science, 537*, 671–681. https://doi.org/10.1016/j.jcis.2018.11.073

Sadaqat, A., Ali, G., Ali, Z., Iftikhar, F. J., Hasan, M., & ul. (2021). Synergetic effect of binary ZnS:SnS composites with reduced graphene oxide and carbon nanotubes as anodes for sodium-ion batteries. *ACS Applied Energy Materials, 4*(12), 13868–13877. https://doi.org/10.1021/acsaem.1c02639

Selvi, S., Rajendran, R., Barathi, D., & Jayamani, N. (2021). Facile synthesis of CeO_2/$CoWO_4$ hybrid nanocomposites for high photocatalytic performance and investigation of antimicrobial activity. *Journal of Electronic Materials, 50*(5), 2890–2902. https://doi.org/10.1007/s11664-020-08729-z

Shanmugam, P., Ngullie, R. C., Meejoo Smith, S., Boonyuen, S., Boddula, R., & Pothu, R. (2023a). Visible-light induced photocatalytic removal of methylene blue dye by copper oxide decorated zinc oxide nanorods. *Materials Science for Energy Technologies, 6*, 359–367. https://doi.org/10.1016/j.mset.2023.03.001

Shanmugam, P., Smith, S. M., Boonyuen, S., & Luengnaruemitchai, A. (2023b). In-situ development of boron doped g-C_3N_4 supported SBA-15 nanocomposites for photocatalytic degradation of tetracycline. *Environmental Research, 224*, 115496. https://doi.org/10.1016/j.envres.2023.115496

Shanmugam, P., Wei, W., Qian, K., Jiang, Z., Lu, J., & Xie, J. (2019). Efficient removal of erichrome black T with biomass-derived magnetic carbonaceous aerogel sponge. *Materials Science and Engineering: B, 248*, 114387. https://doi.org/10.1016/j.mseb.2019.114387

Sivaranjani, T., Rajakarthihan, S., Bharath, G., Haija, M. A., & Banat, F. (2023). An advanced photo-oxidation process for pharmaceuticals using plasmon-assisted Ag-$CoFe_2O_4$ photocatalysts. *Chemosphere, 341*, 139984. https://doi.org/10.1016/j.chemosphere.2023.139984

Subbulakshmi, A., Durgadevi, S., Anitha, S., Govarthanan, M., Biruntha, M., Rameshthangam, P., & Kumar, P. (2023). Biogenic gold nanoparticles from Gelidiella acerosa: Bactericidal and photocatalytic degradation of two commercial dyes. *Applied Nanoscience, 13*(6), 4033–4042. https://doi.org/10.1007/s13204-022-02693-2

Thanigaivel, S., Vickram, S., Manikandan, S., Deena, S. R., Subbaiya, R., Karmegam, N., et al. (2022). Sustainability and carbon neutralization trends in microalgae bioenergy production from wastewater treatment: A review. *Bioresource Technology, 364*, 128057. https://doi.org/10.1016/j.biortech.2022.128057

Thommes, M., & Cychosz, K. A. (2014). Physical adsorption characterization of nanoporous materials: Progress and challenges. *Adsorption, 20*(2), 233–250. https://doi.org/10.1007/s10450-014-9606-z

Venugopal, V., Balaji, D., Preeyanghaa, M., Moon, C. J., Neppolian, B., Muthusamy, G., et al. (2023). Synergistic combination of $BiFeO_3$ nanorods and $CeVO_4$ nanoparticles for enhanced visible light driven photocatalytic activity. *Alexandria Engineering Journal, 72*, 531–543. https://doi.org/10.1016/j.aej.2023.04.024

Vignesh, S., Palanisamy, G., Srinivasan, M., Elavarasan, N., Bhuvaneswari, K., Venkatesh, G., et al. (2021). Fabricating SnO_2 and Cu_2O anchored on g-C_3N_4 nanocomposites for superior photocatalytic various organic pollutants degradation under simulated sunlight exposure. *Diamond and*

Related Materials, 120, 108606. https://doi.org/10.1016/j.diamond.2021.108606

Wang, G., Huang, B., Li, Z., Lou, Z., Wang, Z., Dai, Y., & Whangbo, M.-H. (2015). Synthesis and characterization of ZnS with controlled amount of S vacancies for photocatalytic H2 production under visible light. *Scientific Reports, 5*(1), 8544. https://doi.org/10.1038/srep08544

Wang, X., Zhou, J., Zhao, S., Chen, X., & Yu, Y. (2018). Synergistic effect of adsorption and visible-light photocatalysis for organic pollutant removal over $BiVO_4$/carbon sphere nanocomposites. *Applied Surface Science, 453*, 394–404. https://doi.org/10.1016/j.apsusc.2018.05.073

Xu, W.-T., Ma, L., Ke, F., Peng, F.-M., Xu, G.-S., Shen, Y.-H., et al. (2014). Metal–organic frameworks MIL-88A hexagonal microrods as a new photocatalyst for efficient decolorization of methylene blue dye. *Dalton Transactions, 43*(9), 3792–3798. https://doi.org/10.1039/C3DT52574K

Yan, N., Zhou, Y., Zheng, Y., Qiao, S., Yu, Q., Li, Z., & Lu, H. (2015). Antibacterial properties and cytocompatibility of bio-based nanostructured carbon aerogels derived from silver nanoparticles deposited onto bacterial cellulose. *RSC Advances, 5*(118), 97467–97476. https://doi.org/10.1039/C5RA15485E

Zhang, P., Yin, L., Yang, X., Wang, J., Chi, M., & Qiu, J. (2023a). Cotton-derived 3D carbon fiber aerogel to in situ support Bi_2O_3 nanoparticles as a separation-free photocatalyst for antibiotic removal. *Carbon, 201*, 110–119. https://doi.org/10.1016/j.carbon.2022.09.012

Zhang, Y., Liu, F., Zhong, L., Dong, Z., Chen, C., & Xu, Z. (2023b). Reusable and environmentally friendly cellulose nanofiber/titanium dioxide/chitosan aerogel photocatalyst for efficient degradation of tetracycline. *Applied Surface Science, 641*, 158425. https://doi.org/10.1016/j.apsusc.2023.158425

Zhu, W., Han, M., Kim, D., Zhang, Y., Kwon, G., You, J., et al. (2022). Facile preparation of nanocellulose/Zn-MOF-based catalytic filter for water purification by oxidation process. *Environmental Research, 205*, 112417. https://doi.org/10.1016/j.envres.2021.112417